THE JOURNAL OF PHYSICAL CHEMISTRY Letters

Letter

pubs.acs.org/JPCL

Predicted Optimum Composition for the Glass-Forming Ability of Bulk Amorphous Alloys: Application to Cu–Zr–Al

Qi An,[†] Konrad Samwer,[‡] William A. Goddard, III,*[,†] William L. Johnson,*[,§] Andres Jaramillo-Botero,[†] Glenn Garret,[§] and Marios D. Demetriou[§]

[†]Materials and Process Simulation Center and [§]Keck Engineering Laboratories, California Institute of Technology, Pasadena, California 91125, United States

[‡]I. Physik Institute, University of Goettingen, Goettingen, Germany

Supporting Information

ABSTRACT: Metallic glasses have been established to have unique properties such as ductility, toughness, and soft magnetism with promising engineering applications. However, the glass-forming ability (GFA) has not been sufficient to synthesize the bulk metallic glasses (BMGs) required for many engineering applications. Attempts to develop the understanding of the GFA required to predict the optimum alloys have not yet been proven successful. We develop here a computational model based on molecular dynamics simulations that explains the dramatic change of GFA with alloying small amounts of Al into Cu–Zr. We find that the high GFA to form BMGs depends on a combination of three factors, (a) a low thermodynamic driving force for crystallization, (b) a high melt viscosity, and (c) large ratios of icosahedral structures in the liquid phase. These computational methods to predict these factors that suppress formation of crystal nuclei and slow the dynamic motions in the liquids are practical for in silico prediction of new alloys with optimal GFA.

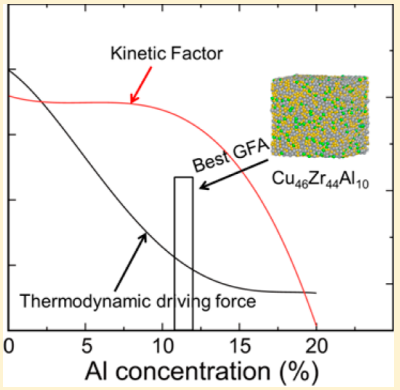

SECTION: Glasses, Colloids, Polymers, and Soft Matter

Metallic glasses have been established to have unique properties such as ductility, high fracture toughness, high corrosion resistance, and soft magnetism.[1−8] Unfortunately, it has been difficult to use these unique properties in a wide range of engineering applications because the need for rapid solidification limits the thickness of the amorphous materials while complicating processing. Great progress has been made toward synthesizing bulk metallic glasses (BMGs) since the first amorphous materials made (in 1960[1]) by rapid solidification at cooling rates of 10^6 K/s to form very thin films. Now, multicomponent metallic glasses with critical sizes larger than 10 mm in diameter have been synthesized with much lower cooling rates ($1-10^3$ K/s).[2−4] Particularly interesting are the Cu–Zr-based BMGs that have the best glass forming ability (GFA) among binary alloys. Most interesting is that additional alloying elements can dramatically improve the GFA, leading to extraordinary mechanical properties and broad engineering applicability.[6,9]

Although GFA plays an essential rule in developing thick BMGs with improved mechanical properties, a fundamental understanding of the factors controlling GFA remains controversial, despite numerous experimental and theoretical studies. Many theories and approaches have been proposed to predict the optimum compositions for glass formation. For example, Turnbull[10] proposed that GFA increases as the reduced glass transition temperature, $T_{rg} = T_g/T_l$, increases, where T_g is the glass transition temperature and T_l is the liquidus or melting temperature. This idea was further extended by Inoue[4] to account for the range of the undercooled liquid regions ($\Delta T_x = T_x - T_g$), where the T_x is the onset temperature for crystal melting. The T_{rg} rule suggested that the best GFA region would be located near the eutectic point of the alloy, but many experimental observations find otherwise.[11,12] Furthermore, this concept would not explain the crystalline phases found to emerge from the glass matrix. Others have hypothesized explanations of GFA based on the concept of the glass phase competing by suppressing crystal growth of all possible crystalline structures.[13,14] In particular, the importance of atomic size ratios and the presence of icosahedral structures in the melt have been emphasized.[15,16]

In this Letter, we use molecular dynamics (MD) simulations to predict the thermodynamic driving forces, the melt viscosity, and the atomic structures as a function of alloying Al into the Cu–Zr binary alloy. In particular, we predict the thermodynamic properties of the liquids and vitreous alloys during the quenching process. These studies predict that the optimum glass formers for Cu–Zr–Al ternary alloys have ∼12.5% Al, which agrees very well with recent experiments[6,17−20] and theories.[6,21−23]

Received: September 17, 2012
Accepted: October 10, 2012
Published: October 10, 2012

   dx.doi.org/10.1021/jz3014425 | J. Phys. Chem. Lett. 2012, 3, 3143–3148

We examine here the properties of glass-forming liquids of the composition of $Zr_{54-x}Cu_{46}Al_x$ (x = 1−25). The details of MD simulations are in the Supporting Information (SI). Figure S1a (SI) shows the potential energy of some selected systems as a function of temperature during the quench process using a cooling rate of 0.5×10^{11} K/s. We use a high cooling rate because the atomic fluctuations require a short MD time step (femtosecond), which limits the simulation time scale for practical calculations to less than microseconds. As the Al concentration increases, the potential energy shifts to a higher level. All curves have a change in slope at around 800 K, which indicates the glass transition from liquid states.

Thermodynamic variables, such as volume, potential energy, enthalpy, and so forth, are continuous during the liquid−glass transition. However, the derivatives of these variables (heat capacity, thermal expansion) can show an abrupt change at T_g. This enables us to predict T_g from the MD. We extract the specific enthalpy (H) directly from simulations via the thermodynamic relation $H = PV + U$, where U is the internal energy, P is the pressure, and V is the volume. We also calculate the specific enthalpy by integrating the specific heat capacity (C_p). Our quenching process covers the liquid, undercooled liquid, and glass regions. For the solid states, classical MD leads to $C_p = 3R$, the Dulong−Petit law, where R is the gas constant. On the basis of previous studies,[24−26] the temperature-dependent specific heat capacity for liquid and undercooled liquid can be expressed as inversely proportional by a power series with an inverse square of the temperature term.

$$C_p = 3R + A \times T + B \times T^{-2} \quad (1)$$

We predict T_g and the prefactor B of $1/T^2$ by fitting the enthalpy as a function of temperature.

The enthalpy of the $Cu_{46}Zr_{44}Al_{10}$ system, as a function of temperature, is shown in Figure 1a. The green line is fitted from eq 1 in the range of 900−2000 K, and the red line is from the Dulong−Petit law in the range of 300−500 K. The glass transition temperature was determined from the intersection of the solid and liquid enthalpy lines. The T_g of other Al concentrations was also extracted in the same manner. The T_g for various Al concentrations is shown in Figure S1b (SI). As the Al concentration increases from 0 to 10%, T_g increases, reaching a maximum at around 10%. Then, it decreases past 15%. The solid black line in this figure corresponds to a second-order polynomial fit, showing the change of T_g as a function of Al concentration.

The prefactor B for $1/T^2$ in the liquid region was also computed and plotted in Figure 1b. The plot of prefactor B versus composition shows a convex curvature for Al concentrations less than 10% with a transition to concave for Al concentrations above 10%. This can be interpreted in terms of two liquid regions with different thermal properties separated at 10%. We fitted the B parameters in the two liquid regions to a second-order polynomial function, leading to the results shown in blue (<10% Al) and green (>10% Al) in Figure 1b.

Energy landscape theory suggests that the thermal properties of undercooled liquids and glasses are related to the potential energy minima.[27−29] The basin enumeration function $\sigma(\varphi)$ is the entropy per particle arising from the existence of multiple minima of depth φ. The enumeration function is often well-represented by a parabola, indicative of a Gaussian distribution of basins. On the basis of the energy landscape model, the excess heat capacity (the difference between the liquid and glass) of metallic glass-forming liquids approaches a $1/T^2$ dependence.[26] Here, the fitting parameter B represents the width parameter of the Gaussian distribution of basins and determines the shape of the enumeration function $\sigma(\varphi)$ (the configuration entropy). The B parameter, as a function of composition shown in Figure 1b, indicates that the potential energy landscape of glass-forming liquids changes much faster as Al is added up to 10% Al; then, it slows for Al concentrations past the phase boundary. Although we cannot relate this liquid change directly with the GFA, the phase boundary of two liquids is close to the best GFA zone. This indicates that the potential energy landscape plays some roles in determining the GFA and provides another way to consider the GFA of different compositions.

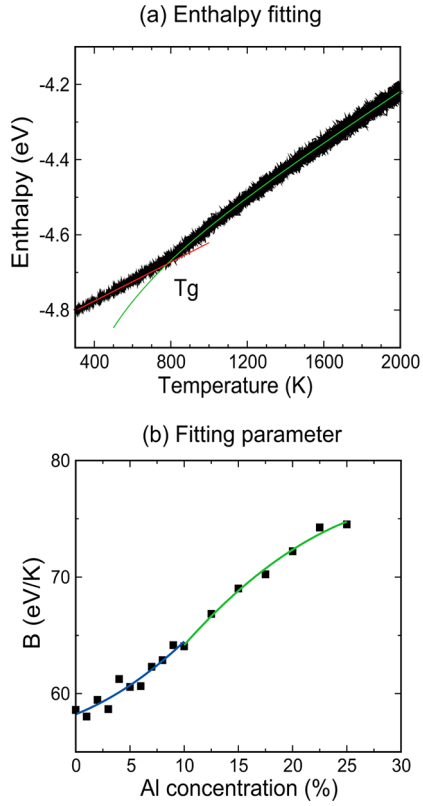

Figure 1. (a) Enthalpy (integration of specific heat capacity) fitting based on the Gaussian model of potential energy landscape theory. (b) Fitting parameters B for various Al concentrations. The blue curves are fitted to a quadratic function ($f(x) = ax^2 + bx + c$) from 0 to 10% Al, while the green curve is fitted to 10−25%. The fitting parameters are a_1 = 0.026, b_1 = 0.367, and c_1 = 58.245 for the blue curve and a_2 = −0.018, b_2 = 1.313, and c_2 = 53.195 for the green curve.

To obtain the thermodynamic driving force for crystallization, we extracted the free energy of the crystal phases and liquid phases using the two-phase thermodynamics (2PT) density of states model which provides accurate free energies and entropies from short MD trajectories.[30−37] The details of the 2PT model and the free-energy approach for the liquid and mixed crystal phases are in the SI. Figure 2a shows the free energy of the various phases, including the crystal phases and liquid phases for various Al concentrations. The common tangent rule was applied to extract the free energy of mixing crystal phases from the three crystal structures. Then, ΔG was obtained by the free-energy difference of liquid and mixing

dx.doi.org/10.1021/jz3014425 | J. Phys. Chem. Lett. 2012, 3, 3143−3148

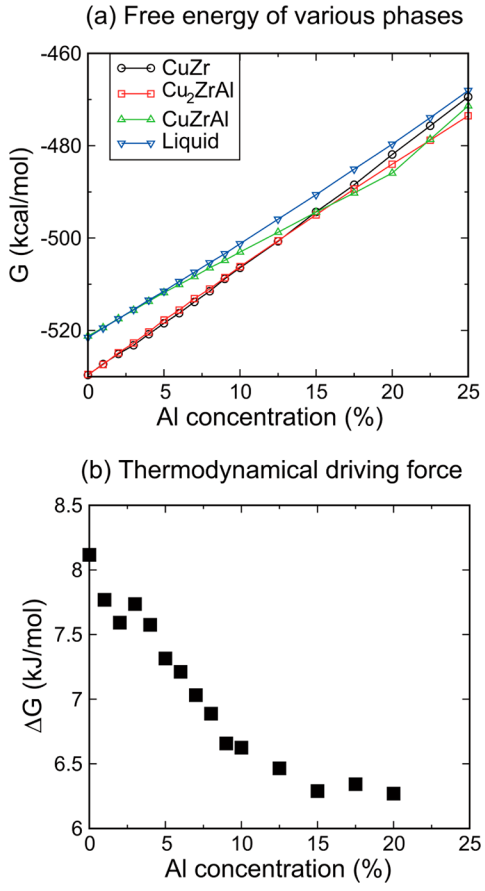

Figure 2. (a) Free energy of various phases (liquids and three crystal phases) from 2PT calculations. (b) Thermodynamic driving force of glass-forming liquids at T = 800 K (just above T_g) calculated from the free-energy difference of the liquid phase and mixing crystal phase. It decreases to a constant value for an Al concentration above ∼12.5%.

crystal phases, as shown in Figure 2b. The thermodynamic driving force decreases as the Al concentration increases and then becomes constant when the Al concentration passes through 12.5%, indicating a better GFA region with an Al% concentration higher than 12.5%.

Viscosity plays an essential role in glass-forming liquids because it determines the α-relaxation time for undercooled liquids. [The α-relaxation ceases when T approaches T_g, while the β-relaxation process persists into the glassy state.] An increase of viscosity decreases the atomic diffusivity, making it hard for the system to find the optimal atomic rearrangement for crystallization. An important parameter here is the nose temperature, which is defined by the minimum crystallization time in the time−temperature transformation (TTT) diagram. Previous studies[38] found that the melt viscosity at the nose temperature is the significant factor determining the GFA. The nose temperature is typically ∼100−200 K higher than T_g.[38] Here, we measured the melt viscosities of undercooled liquids based on R-NEMD studies in ref 39 at T = 1000 K, which is estimated to be the nose temperature for various Al concentrations. We also computed the temperature-dependent viscosities of three typical Al concentrations (5%, 10, and 20%) from 900 to 1500 K. The details of viscosity calculations from MD simulations and R-NEMD methods are in the SI.

Figure S2 (SI) shows the viscosity as a function of the shear strain rate for $Cu_{46}Zr_{44}Al_{10}$ at T = 1000 K. The shear viscosity decreases with higher shear strain rates, showing a shear-thinning behavior. The red line is fit with the Curreau equation[40]

$$\eta(\dot{\gamma}) = \frac{\eta_0}{(1 + (\lambda\dot{\gamma})^2)^{\alpha}} \quad (2)$$

where $\dot{\gamma}$ is the shear rate. It shows that the metallic liquid is a Newtonian fluid for shear strain rates smaller than 0.5×10^{-3} per ps. We find a Newtonian viscosity of 27.8 cP from the fit. The melt viscosities for various Al concentrations were also extracted using the same approach, leading to the results shown in Figure 3a.

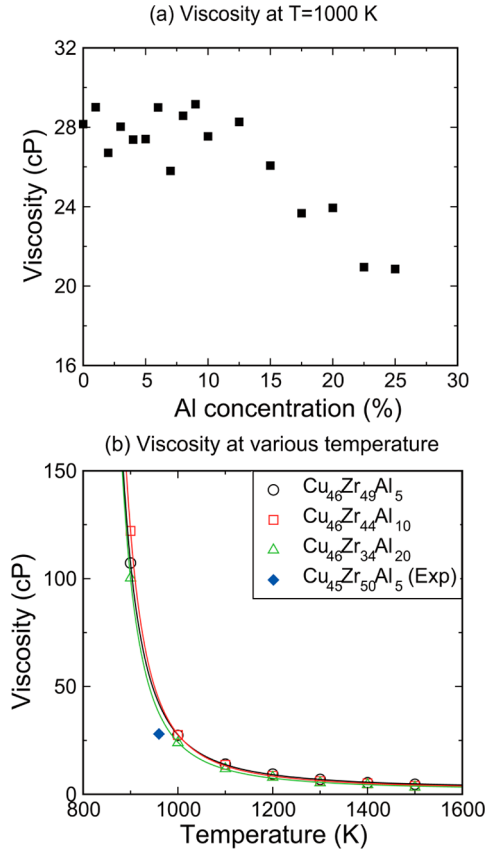

Figure 3. Dynamical viscosity from R-NEMD calculations over the temperatures range of 900−1500 K for various Al compositions. (a) Viscosity for various Al concentrations at T = 1000 K. The melt viscosity is constant below 12.5% Al and decreases at higher concentrations of 25% Al. The melt viscosity is 30% below the low Al values. (b) Temperature dependence of viscosity for selected Al concentrations. The curve for 10% Al is stiffer than the other two cases. Experimental data are from ref 43.

We see that the melt viscosities remain constant as the Al concentration increases until ∼12.5% composition and then drop past this point. The viscosity finally drops 30% as the Al concentration reaches 25%. Thus, on the basis of viscosity, we expect the good GFA in the region with an Al concentration lower than 12.5%.

We also investigated the temperature-dependent dynamic viscosity for some typical Al concentrations (5, 10, and 20%) based on R-NEMD at temperatures from 900 to 1500 K. These results are shown in Figure 3b. The temperature-dependent

dx.doi.org/10.1021/jz3014425 | J. Phys. Chem. Lett. 2012, 3, 3143−3148

dynamic viscosities can be described by the Vogel−Fulcher−Tammann (VFT) equation

$$\eta = \eta_0 \times \exp\left[D \times \frac{T_0}{T - T_0}\right] \quad (3)$$

where T_0 is referred to as the VFT temperature, D is known as the fragility parameter, and η_0 is the high-temperature limit of viscosity. The viscosity fitting parameters of three alloys at various Al concentrations are listed in Table S1 (SI). We see that the 10% Al concentration has the highest viscosity when the temperature is lower than 1100 K and that the slope of the curve becomes much stiffer as the temperature approaches T_g. This indicates a much higher viscosity for 10% Al liquids than the other two cases when approaching T_g.

On the basis of classical nucleation theory, the activation barrier for crystallization in the undercooled liquid is $\Delta G^* = 16\pi\sigma^3/(3\Delta G^2)$, where σ is the interfacial energy of the critical nuclei and ΔG is the thermodynamical driving force. Thus, a low thermodynamical driving force (ΔG) and a high interfacial energy lead to the improved BMG stability. On the other hand, from a kinetics viewpoint, a viscous liquid should have high viscosity in order to deter the crystallization and realize the high GFA of vitreous alloys. Figure 2b shows that the lowest ΔG occurs above 12.5% Al, while Figure 3a shows that the largest dynamic viscosity occurs for Al less than 12.5%. These results indicate that the best GFA region is ∼12.5% Al.

To understand how the local atomic configurations might affect the GFA, we examined the undercooled glass-forming liquid structure at 800 K for various Al concentrations and characterized them in terms of a Voronoi analysis,[41] which partitions space in terms of Voronoi polyhedra (VP) containing all points closer to an atom than to any other atoms. Here, each VP is represented by the indexes (f_3, f_4, f_5, f_6) corresponding to the number of triangular, tetragonal, pentagonal, and hexagonal faces. Taking Cu and Zr as the polyhedral centers, we examined the VPs related to GFA. For Cu-centered polyhedral, we considered polyhedral such as (0, 0, 12, 0), which is typical of an icosahedral structure, and we considered (0, 2, 8, 2) and (0, 1, 10, 2), indicating the distorted icosahedral structures. In contrast, fcc and hcp would lead to (0, 12, 0, 0), while bcc would lead to (0, 6, 0, 8). We also examined the Zr-centered polyhedral (0, 1, 10, 4) and (0, 1, 10, 5), which are believed to relate to the slowness of liquid motions in Cu−Zr−Al ternary metallic liquids.[42]

The Voronoi analysis results for undercooled liquids of various Al concentrations are shown in Figure 4. The Cu-centered (0, 0, 12, 0) index increases abruptly as the Al concentration increases from 0 to 10% and remains constant above 10% Al. Cu-centered (0, 2, 8, 2) and Zr-centered (0, 1, 10, 4) show a similar but less pronounced increase. These results indicate that the icosahedral structure is the most important structure determining the GFA[16] and that the liquid structure around T_g becomes more stable when the Al concentration is higher than 10%.

Our Voronoi analyses in Figure 4 also indicate two liquid regions having different structural character, which is consistent with the thermodynamic properties that indicate a correlation of the structure and potential energy landscape. For Al concentrations less than 10%, the Cu-centered icosahedral indexes increase proportionally as the Al component increases, while they remain almost constant for Zr-centered icosahedra. For Al concentration > 10%, the Cu-centered icosahedral

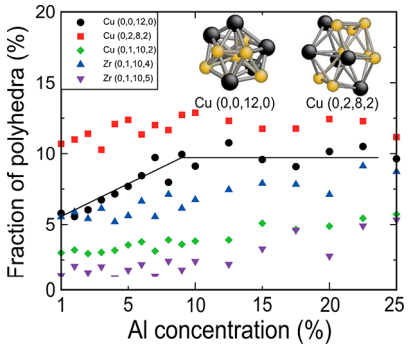

Figure 4. Voronoi polyhedron analyses at glass transition temperatures for various Al concentrations. The icosahedron (0, 0, 12, 0) increases dramatically when the Al concentration is less than 10%, reaching a constant when Al is greater than 10%. The insets are the Cu-centered (0, 0, 12, 0) and (0, 2, 8, 2) polyhedra, where the yellow represents the Cu atom and the black represents the Zr atom. Other abundant VPs in the undercooled liquids include (0, 3, 6, 4), (0, 2, 8, 1), (0, 2, 8, 4), and (0, 3, 6, 3), which are 6.2, 5.9, 5.0, and 4.3%, respectively, in $Cu_{46}Zr_{44}Al_{10}$ liquids at T_g. The other small fraction of less than 4% VPs is over 20 types. The solid black line is to help view the icosahedron ratios as a function of Al concentration.

indexes change little with respect to the increase of Zr-centered indexes. Because the Al atom radius (1.25 Å) is less than the Zr atom radius (1.55 Å), but close to the Cu atom radius (1.35 Å), we expect the icosahedral structures to form easily as the Al concentration increases. However, when Al is above 10%, we observe a nearly constant number of icosahedral structures, indicating that the GFA decreases as Al increases from 10 to 25%. These results are consistent with the previous analyses of the thermodynamic driving force and viscosity, indicating that the best GFA is at around 10−12.5% Al.

The results presented in Figure S1b (SI) and Figure 1b show that the ternary Cu−Zr−Al glass-forming liquid properties are composition-dependent. The behavior of T_g and the fitting parameter B from eq 1 are quite different for Al less than 10% compared to those for Al above 10%. These results indicate that the composition change in the two regions may play different roles in the GFA and may also affect the mechanical or thermal properties of BMGs at room temperature. The calculations of thermodynamic driving force and melt viscosity show that the best GFA region is around 12.5% Al, which is very close to the phase boundary of two liquids. The structure analyses for the various glass-forming liquids around T_g confirmed that the two liquid regions cross at 10% Al. Thus, taken together, our co-locations indicate that the best GFA region is at 10−12.5% Al.

As the Al component increases from 0 to 25% (substituting for Zr atoms), we find that the liquid-phase regions lead to two distinctly different tendencies in the potential energy landscape, the icosahedral structure ratios, the melt viscosity, and the thermodynamic driving force. The combination of melt viscosities, thermodynamic driving force, and icosahedral structures in glass-forming liquids suggests that the best GFA region is at 10−12.5% Al. These predictions are consistent with experimental data extracted from the contour map of the experiment,[22] showing that the best GFA region (along the line examined here) is 9−12% Al. Figure S3 (SI) compares the experimental results to our predictions for replacing Zr with Al while fixing the Cu atom concentration, which corresponds to the line in the ternary phase diagram.

dx.doi.org/10.1021/jz3014425 | J. Phys. Chem. Lett. 2012, 3, 3143−3148

Summarizing, the high GFA from adding 12.5% Al to Zr-based BMGs is a direct result of (1) an increased melt viscosity, which slows the dynamical motion of the liquids; (2) a decreased thermodynamic driving force that suppresses crystal nucleation; and (3) high ratios of icosahedron structures that stabilize the liquid structure at around T_g. These three factors prevent the liquid from crystallizing and improve the GFA of BMGs.

On the basis of this examination of GFA for the current Cu–Zr–Al system, we suggest that the combination of melt viscosity, thermodynamic driving force, and icosahedral structure ratios could be used to predict the optimum combinations of ternary alloys for the best GFA. Such MD simulations could be used to discover optimum glass formers for a complex ternary phase diagram prior to costly experimental synthesis and characterization. We consider that our model combining the melt viscosity, the thermodynamic driving force, and the amount of icosahedral character is sufficiently general that it could serve for examining the GFA of other potential BMGs. Interesting applications include extending our analysis to Fe-based and Pd-based metallic glasses.

■ ASSOCIATED CONTENT

Ⓢ Supporting Information

Details of the MD simulation, the method of obtaining the thermodynamic driving force from the 2PT model, the approaches to extract dynamical viscosity from MD, and the structure analyses with Voronoi tessellation. Also, the figures include the thermodynamic properties of liquids and glass during the quenching process for various Al concentrations, the dynamical viscosity as a function of strain rate for undercooled liquids, and the comparison of GFA between experiment and simulations. The table includes the viscosity fitting parameters from the VFT equation. This material is available free of charge via the Internet at http://pubs.acs.org.

■ AUTHOR INFORMATION

Corresponding Author

*E-mail: wag@wag.caltech.edu (W.A.G.); wlj@caltech.edu (W.L.J.).

Notes

The authors declare no competing financial interest.

■ ACKNOWLEDGMENTS

All computations were carried out on the SHC computers (Caltech Center for Advanced Computing Research) provided by the Department of Energy National Nuclear Security Administration PSAAP project at Caltech (DE-FC52-08NA28613) and by the NSF DMR-0520565 CSEM computer cluster. A.J.B. and W.A.G. received support from the PSAAP while A.Q, W.A.G., W.L.J., G.G., and M.D.D. thank NSF DMR-0520565 Caltech CSEM for support. K.S. is grateful for support by the DFG via the SFB 602 and the Leibniz-Program.

■ REFERENCES

(1) Klement, W.; Willens, R. H.; Duwez, P. Non-crystalline Structure in Solidified Gold-Silicon Alloys. *Nature* **1960**, *187*, 869–870.
(2) Greer, A. L. Metallic Glasses. *Science* **1995**, *267*, 1947–1953.
(3) Johnson, W. L. Bulk Glass-Forming Metallic Alloys: Science and Technology. *Mater. Res. Bull.* **1999**, *24*, 42–56.
(4) Inoue, A. Stabilization of Metallic Supercooled Liquid and Bulk Amorphous Alloys. *Acta Mater.* **2000**, *48*, 279–306.
(5) Lu, Z. P.; Lu, C. T; Thompson, J. R.; Porter, W. D. Structural Amorphous Steels. *Phys. Rev. Lett.* **2004**, *93*, 245503.
(6) Xu, D. H.; Duan, G; Johnson, W. L. Unusual Glass-Forming Ability of Bulk Amorphous Alloys Based on Ordinary Metal Copper. *Phys. Rev. Lett.* **2004**, *92*, 245504.
(7) Ponnambalam, V.; Poon, S. J.; Shiflet, G. J. Fe-based Bulk Metallic Glasses with Diameter Thickness Larger than One Centimeter. *J. Mater. Res.* **2004**, *19*, 1320–1323.
(8) Wang, W. H.; Dong, C.; Shek, C. H. Bulk Metallic Glasses. *Mater. Sci. Eng. Res.* **2004**, *44*, 45–89.
(9) Cheng, Y. Q.; Cheng, Ma. E.; Sheng, H. W. Alloying Strongly Influences the Structure, Dynamics, and Glass Forming Ability of Metallic Supercooled Liquids. *Appl. Phys. Lett.* **2008**, *93*, 111913.
(10) Turnbull, D. Under what Conditions Can a Glass Be Formed? *Contemp. Phys.* **1969**, *10*, 473–488.
(11) Chen, H. S. Glassy Metals. *Rep. Prog. Phys.* **1980**, *43*, 353–432.
(12) Tan, H.; Zhang, Y.; Ma, D.; Feng, Y. P.; Li, Y. Optimum Glass Formation at Off-Eutectic Composition and its Relation to Skewed Eutectic Coupled Zone in the La Based La–Al–(Cu,Ni) Pseudo Ternary System. *Acta Mater.* **2003**, *51*, 4551–4561.
(13) Ma, D.; Change, Y. A. Competitive Formation of Ternary Metallic Glasses. *Acta Mater.* **2006**, *54*, 1927–1934.
(14) Ma, D.; Tan, H.; Wang, D.; Li, Y.; Ma, E. Strategy for Pinpointing the Best Glass-Forming Alloys. *Appl. Phys. Lett.* **2005**, *86*, 191906.
(15) Qi, Y.; Cagin, T.; Kimura, Y.; Goddard, W. A., III. Molecular Dynamics Simulations of Glass Formation and Crystallization in Binary Liquid Metals: Cu–Ag and Cu–Ni. *Phys. Rev. B* **1999**, *59*, 3527–3533.
(16) Lee, H. J.; Cagin, T.; Johnson, W. L.; Goddard, W. A., III. Criteria for Formation of Metallic Glasses: The Role of Atomic Size Ratio. *J. Chem. Phys.* **2003**, *119*, 9858–9870.
(17) Wang, D.; Tan, H.; Li, Y. Multiple Maxima of GFA in Three Adjacent Eutectics in Zr–Cu–Al Alloy System — A Metallographic Way to Pinpoint the Best Glass Forming Alloys. *Acta Mater.* **2005**, *53*, 2969–2979.
(18) Inoue, A.; Negishi, T.; Kimura, H. M.; Zhang, T.; Yavari, A. R. High Packing Density of Zr- and Pd-Based Bulk Amorphous Alloys. *Mater. Trans., JIM* **1998**, *39*, 318–321.
(19) Yokoyama, Y.; Inoue, H.; Fukaura, K.; Inoue, A. Relationship Between the Liquidus Surface and Structures of Zr–Cu–Al Bulk Amorphous Alloys. *Mater. Trans.* **2002**, *43*, 575–579.
(20) Bo, H.; Wang, J.; Lin, S.; Qi, H. Y.; Yuan, X. L.; Liu, L. B.; Jin, Z. P. Thermodynamic Analysis of the Al–Cu–Zr Bulk Metallic Glass System. *Intermetallics* **2010**, *18*, 2322–2327.
(21) Angell, C. A. Glass-Formers and Viscous Liquid Slowdown since David Turnbull: Enduring Puzzles and New Twists. *MRS Bull.* **2008**, *33*, 544–555.
(22) Oliveira, M. F. A Simple Criterion to Predict the Glass Forming Ability of Metallic Alloys. *J. Appl. Phys.* **2012**, *111*, 023509.
(23) Zhang, G. Y.; An, Q.; Goddard, W. A., III. Composition Dependence of Glass Forming Propensity in Al–Ni Alloys. *J. Phys. Chem. C* **2011**, *115*, 2320–2331.
(24) R. Busch, R.; Kim, Y. J.; Johnson, W. L. Thermodynamics and Kinetics of the Undercooled Liquid and the Glass Transition of the $Zr_{41.2}Ti_{13.8}Cu_{12.5}Ni_{10.0}Be_{22.5}$ Alloy. *J. Appl. Phys.* **1995**, *77*, 4039–4043.
(25) Kubaschewski, O.; Alcock, C. B.; Spencer, P. J. *Materials Thermochemistry*, 6th ed.; Pergamon: New York, 1993.
(26) Johnson, W. L.; Kaltenboeck, G.; Demetriou, M. D.; Schramm, J. P.; Liu, X.; Samwer, K.; Kim, C. P.; Hofmann, D. C. Beating Crystallization in Glass-Forming Metals by Millisecond Heating and Processing. *Science* **2011**, *332*, 828–833.
(27) Debenedetti, P. G.; Stillinger, F. H.; Truskett, T. M; Lewis, C. P. Theory of Supercooled Liquids and Glasses: Energy Landscape and Statistical Geometry Perspectives. *Adv. Chem. Eng.* **2001**, *28*, 21–79.
(28) Sciortino, F.; Kob., W; Tartaglia, P. Inherent Structure Entropy of Supercooled Liquids. *Phys. Rev. Lett.* **1999**, *83*, 3214–3217.
(29) Speedy, R. J. Relations between a Liquid and Its Glasses. *J. Phys. Chem. B* **1999**, *103*, 4060–4065.

(30) Lin, S. T.; Blanco, M.; Goddard, W. A., III. The Two-Phase Model for Calculating Thermodynamic Properties of Liquids from Molecular Dynamics: Validation for the Phase Diagram of Lennard-Jones Fluids. *J. Chem. Phys.* **2003**, *119*, 11792.
(31) Pascal, T. A.; Lin, S. T.; Goddard, W. A., III. Thermodynamics of Liquids: Standard Molar Entropies and Heat Capacities of Common Solvents from 2PT Molecular Dynamics. *Phys. Chem. Chem. Phys.* **2011**, *13*, 169−181.
(32) Li, Y. Y.; Lin, S. T.; Goddard, W. A., III. Efficiency of Various Lattices from Hard Ball to Soft Ball: Theoretical Study of Thermodynamic Properties of Dendrimer Liquid Crystal from Atomistic Simulation. *J. Am. Chem. Soc.* **2004**, *126*, 1872−1885.
(33) Lin, S. T.; Maiti, P. K.; Goddard, W. A., III. Dynamics and Thermodynamics of Water in PAMAM Dendrimers at Subnanosecond Time Scales. *J. Phys. Chem. B* **2005**, *109*, 8663−8672.
(34) Huang, S. N.; Pascal, T. A.; Goddard, W. A., III; Maiti, P.; Lin, S. T. Absolute Entropy and Energy of Carbon Dioxide Using the Two-Phase Thermodynamic Model. *J. Chem. Theory Comput.* **2011**, *7* (6), 1893−1901.
(35) Pascal, T. A.; Boxe, C.; Goddard, W. A., III. An Inexpensive, Widely Available Material for 4 wt % Reversible Hydrogen Storage near Room Temperature. *J. Phys. Chem. Lett.* **2011**, *2*, 1417−1420.
(36) Pascal, T. A.; Goddard, W. A., III; Jung, Y. Entropy and the Driving Force for the Filling of Carbon Nanotubes with Water. *Proc. Natl. Acad. Sci. U.S.A.* **2011**, *108*, 11794−11798.
(37) Pascal, T. A.; He, Y.; Jiang, S. Y.; Goddard, W. A., III. Thermodynamics of Water Stabilization of Carboxybetaine Hydrogels from Molecular Dynamics Simulations. *J. Phys. Chem. Lett.* **2011**, *2*, 1757−1760.
(38) Mukherjee, S.; Schroers, J.; Johnson, W. L.; Rhim, W. K. Influence of Kinetic and Thermodynamic Factors on the Glass-Forming Ability of Zirconium-Based Bulk Amorphous Alloys. *Phys. Rev. Lett.* **2005**, *94*, 245501.
(39) Muller-Plathe, F. Reversing the Perturbation in Nonequilibrium Molecular Dynamics: An Easy Way to Calculate the Shear Viscosity of Fluids. *Phys. Rev. E* **1999**, *59*, 4894−4898.
(40) Tenney, C. M.; Maginn, E. J. Limitations and Recommendations for the Calculation of Shear Viscosity Using Reverse Nonequilibrium Molecular Dynamics. *J. Chem. Phys.* **2010**, *132*, 014103.
(41) Brostow, W.; Chybicki, M.; Laskowski, R.; Rybicki, J. Voronoi Polyhedra and Delaunay Simplexes in the Structural Analysis of Molecular-Dynamics-Simulated Materials. *Phys. Rev. B* **1998**, *57*, 13448−13458.
(42) Peng, H. L.; Li, M. Z.; Wang, W. H.; Wang, C. Z.; Ho, K. M. Effect of Local Structures and Atomic Packing on Glass Forming Ability in Cu_xZr_{100-x} Metallic Glasses. *Appl. Phys. Lett.* **2010**, *96*, 021901.
(43) Yokoyama, Y.; Ishikawa, T.; Okada, J. T.; Watanabe, Y.; Nanao, S.; Inoue, A. Volume and Viscosity of Zr−Cu−Al Glass-Forming Liquid Alloys. *J. Non-Cryst. Solids* **2009**, *355*, 317−322.